Received: 6 February 2020 | Revised: 19 June 2020 | Accepted: 23 June 2020

DOI: 10.1002/ardp.202000027

FULL PAPER

DPhG ARCH PHARM
Archiv der Pharmazie

Design, synthesis, and biological evaluation of new pyrazoloquinazoline derivatives as dual COX-2/5-LOX inhibitors

Mohamed A. Shaaban[1] | Aliaa M. Kamal[1,2] | Samar I. Faggal[1] | Nahla A. Farag[3] | Nora M. Aborehab[4] | Ayman E. Elsahar[5] | Khaled O. Mohamed[1]

[1]Department of Pharmaceutical Organic Chemistry, Faculty of Pharmacy, Cairo University, Cairo, Egypt

[2]Department of Organic Chemistry, Faculty of Pharmacy, October University for Modern Science and Arts (MSA), Giza, Egypt

[3]Department of Pharmaceutical Chemistry, Faculty of Pharmacy, Misr International University, Cairo, Egypt

[4]Department of Biochemistry, Faculty of Pharmacy, October University for Modern Science and Arts (MSA), Giza, Egypt

[5]Department of Pharmacology and Toxicology, Faculty of Pharmacy, Cairo University, Cairo, Egypt

Correspondence
Khaled O. Mohamed, Department of Pharmaceutical Organic Chemistry, Faculty of Pharmacy, Cairo University, 33 Kasr El-Aini Street, Cairo 11562, Egypt.
Email: khaled.mohamed@pharma.cu.edu.eg

Nahla A. Farag, Department of Pharmaceutical Chemistry, Faculty of Pharmacy, Misr International University, Km 28 Cairo-Ismailia Road (Ahmed Orabi District), Cairo 11431, Egypt.
Email: nahla.farag@miuegypt.edu.eg

Abstract

A new series of pyrazoloquinazoline derivatives equipped with different chalcones was designed, synthesized, and identified through ^{1}H nuclear magnetic resonance (NMR), ^{13}C NMR, and infrared spectroscopic techniques. Our design strategy of the quinazolinone-privileged scaffold as a new scaffold was based on merging pharmacophores previously reported to exhibit cyclooxygenase-2 (COX-2)/5-lipoxygenase (5-LOX) inhibitory activity. All the newly synthesized derivatives were biologically evaluated for COX and 5-LOX inhibitory activity and COX-2 selectivity, using celecoxib and zileuton as reference drugs, as they exhibited promising anti-inflammatory activity. Compound **3j** was found to be the most promising derivative, with IC_{50} values of 667 and 47 nM against COX-1 and COX-2, respectively, which are superior to that of celecoxib (IC_{50} value against COX-2 = 95 nM), showing an SI of 14.2 that was much better than celecoxib. Compounds **3f** and **3h** exhibited COX-1 inhibition, with IC_{50} values of 1,485 and 684 nM, respectively. The synthesized compounds showed a significant inhibitory activity against 5-LOX, with IC_{50} values ranging from 0.6 to 4.3 μM, where compounds **3f** and **3h** were found to be the most potent derivatives, with IC_{50} values of 0.6 and 1.0 μM, respectively, in comparison with that of zileuton (IC_{50} = 0.8 μM). These promising derivatives, **3f**, **3h**, and **3j**, were further investigated in vivo for anti-inflammatory, gastric ulcerogenic effects, and prostaglandin production (PGE2) in rat serum. The molecular docking studies concerning the binding sites of COX-2 and 5-LOX revealed similar orientation, compared with reported inhibitors, which encouraged us to design new leads targeting COX-2 and 5-LOX as dual inhibitors, as a new avenue in anti-inflammatory therapy.

KEYWORDS

5-LOX, anti-inflammatory, COX-2 inhibitors, prostaglandin E2, pyrazolo[5,1-*b*]quinazoline

1 | INTRODUCTION

Inflammation is a multifactorial process; it reflects the response of the organism to various stimuli and is related to many disorders such as rheumatoid arthritis, asthma, psoriasis, and multiple sclerosis, which require prolonged or repeated treatment.[1] Cyclooxygenase (COX) and lipoxygenase (LOX) produce two groups of arachidonic acid metabolites, prostaglandins (COX products) and leukotrienes (LOX products), which play a key role in inflammation.[2–4] The COX-2 expression is induced by pro-inflammatory stimuli and it

generates inflammatory signaling prostaglandins (PGs). COX-2 inhibition is responsible for the anti-inflammatory effect, whereas COX-1 is constitutively active and is responsible for mucus formation in the gastrointestinal tract (GIT), regulation of platelet aggregation, and renal function maintenance. COX-1 inhibition is blamed for inducing GI irritation, the main undesired side effect of nonsteroidal anti-inflammatory drugs (NSAIDs).[5,6] It is important to note that selective COX-2 inhibitors gained much popularity in the late 1990s and early 2000s as anti-inflammatory agents that exhibited minimal GIT side effects.[7] This is attributed to the fact that the binding site of COX-2 enzymes possesses an additional secondary pocket, which is absent in the COX-1 enzyme. This secondary pocket is due to the replacement of amino acid Ile523 in COX-1 with the less bulky Val523 in COX-2.[8] Hence, selective COX-2 inhibitors usually contain bulky rigid groups that allow for additional binding interactions inside COX-2 secondary pocket and prevent the compound to fit inside the narrower COX-1 channel. This additional binding interaction of the inhibitor is thought to be responsible for the selectivity of COX-2 inhibitors.[9] Thus, selective COX-2 inhibitors focus on bicyclic and tricyclic templates, such as celecoxib,[10,11] quinazolinone core-based COX-2 inhibitors **I** and **II**,[12–14] and natural quinazolines such as rutaecarpine[15,16] and tryptanthrin[17,18] (Figure 1). However, clinical practice has proved that not only COX-2 inhibition is associated with cardiovascular side effects, but it is also a dual COX-1/COX-2 inhibition.[19–21] Moreover, blocking only COX-2 will shunt the inflammatory pathway toward LOX pathway, which will hence lead to more side effects due to the production of leukotrienes, lipid mediators, that play a role in inflammation. They are associated with leukocyte activation and adhesion to vascular endothelium,[22] and they are involved in the pathogenesis of bronchial asthma and edema formation.[23] It is also believed that they play a role in the damage of gastric mucosa.[24–26] Therefore, compounds that combine COX-2 and 5-LOX inhibition present multiple advantages, because they act on the two major arachidonic acid metabolic pathways and possess a wide range of anti-inflammatory activity.[27] Recently, Moussa et al.[28] reported a number of thioquinazolinones **III** as well as celecoxib for COX-1/COX-2 and LOX inhibition (Figure 1). In contrast, chalcone moiety has been found to be a privileged pharmacophore that has demonstrated a promising effect in potentiating anti-inflammatory activity.[29,30] Hofmann et al.[31] reported the synthesis of 4′-methoxybenzylidene derivative **IV** as a potential 5-LOX inhibitor, whereas 3,4-dihydroxychalcones showed a dual COX-2/5-LOX inhibition.[32] Therefore, the rational development of chemical structures consisting of fragments that are able to inhibit COX-2 and 5-LOX has nowadays become a highly interesting field of research, which promises better anti-inflammatory efficacy and lower incidences of side effects.

Inspired by these findings, and seeking studies on quinazolinones as promising scaffolds, our strategy focused on designing novel

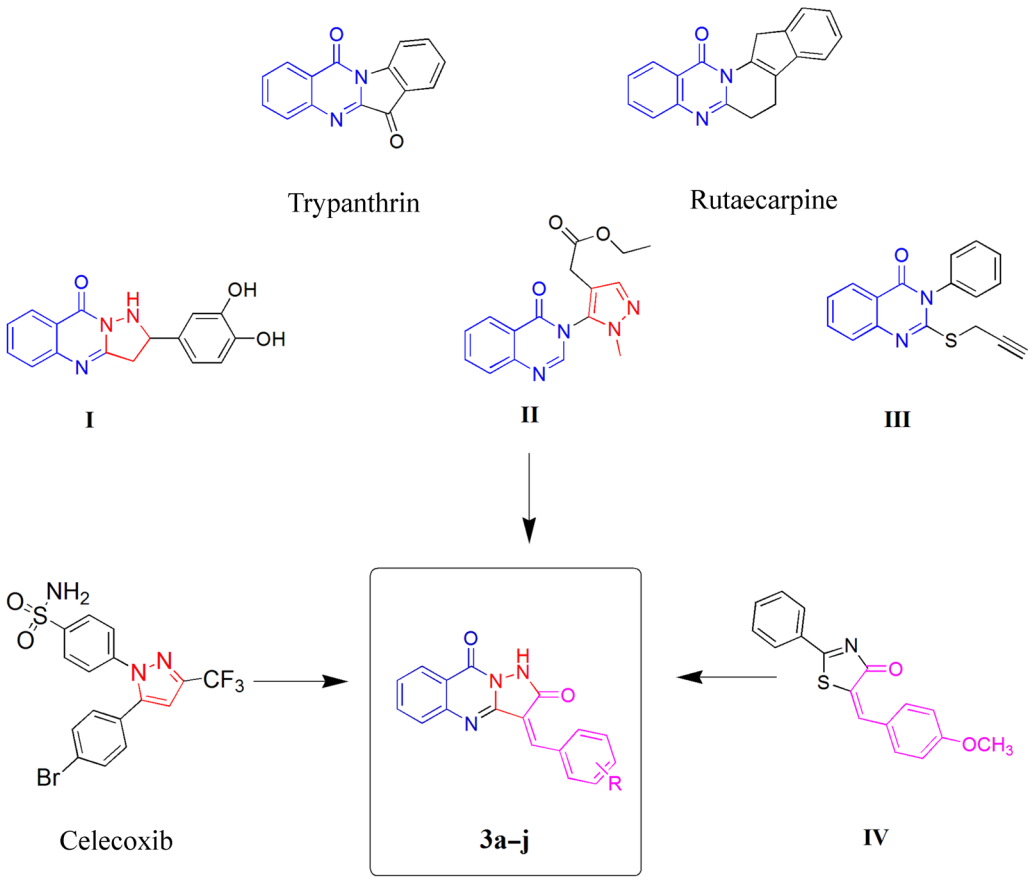

FIGURE 1 The design strategy for the pyrazoloquinazoline- derivatives as dual COX-2/5-LOX inhibitors

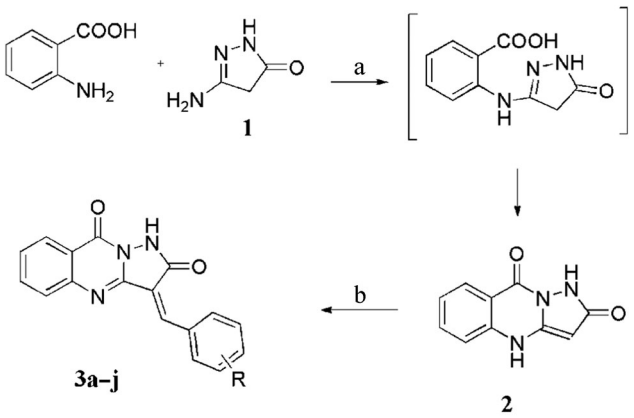

	R
3a	H
3b	2-F
3c	3-F
3d	4-F
3e	2-OCH_3
3f	4-OCH_3
3g	4-Cl
3h	3,4-$(OCH_3)_2$
3i	4-Br
3j	3,4,5-$(OCH_3)_3$

SCHEME 1 The synthetic pathway and reagents for the preparation of target compounds **3a–j**. Reagents and conditions: (a) HCl, H_2O, reflux, 3 hr; (b) aromatic aldehyde, glacial acetic acid, reflux, 5 hr

COX-2/5-LOX inhibitors, based on novel pyrazoloquinazoline nucleus equipped with a variety of chalcone derivatives. The benzylidene ring would be unsubstituted or substituted with a diverse array of groups offering various electronic and lipophilic environments, aiming that the potency and selectivity toward COX-2 and 5-LOX might be improved by varying the substitution pattern of the benzylidene ring.

The synthesized compounds were initially tested for their in vitro COX-1/COX-2 inhibition, followed by the in vivo anti-inflammatory activity, gastric ulcerogenic activity, and subsequent evaluation of PG production for the pyrazoloquinazoline derivatives with the highest selectivity on COX-2 isoform. Furthermore, all the synthesized derivatives were assayed in vitro for their 5-LOX inhibition.

2 | RESULTS AND DISCUSSION

2.1 | Chemistry

The synthetic route to the intermediate **2** and targeted compounds **3a–j** is illustrated in Scheme 1. The starting compound, 3-amino-1*H*-pyrazol-5(4*H*)-one **1**, was prepared according to previously reported procedures.[33] Pyrazolo[5,1-*b*]quinazoline-2,9(1*H*,4*H*)-dione **2** represents the key intermediate for the synthesis of 3-arylidenepyrazolo[5,1-*b*]quinazoline-2,9(1*H*,3*H*)-dione derivatives **3a–j**. Compound **2** was synthesized via reaction of **1** with an equimolar amount of anthranilic acid in water acidified with hydrochloric acid for 3 hr; the formation of

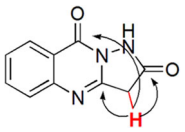

FIGURE 2 The heteronuclear multiple bond correlation of compound **2**

compound **2** was assumed to proceed via the formation of 2-[(4,5-dihydro-5-oxo-1*H*-pyrazol-3-ylamino)] benzoic acid. Interestingly, a novel cyclic structure, pyrazolo[5,1-*b*]quinazoline-2,9(1*H*,4*H*)-dione **2**, was produced, where N2 of pyrazolone ring underwent a spontaneous intramolecular cyclization with the carboxylic acid group of anthranilic acid, followed by dehydration to give a new quinazolone ring instead of benzoic acid derivative. The new cyclic unexpected compound **2** was structurally elucidated on the basis of spectral data as well as microanalysis (infrared [IR], ^{1}H nuclear magnetic resonance [NMR], ^{13}C NMR, heteronuclear multiple bond correlation [HMBC], and mass spectrometry [MS]). The IR spectrum for compound **2** showed the absence of broad OH peak of carboxylic acid that is attributed to the open structure and revealed a band at 3,201 cm^{-1}, corresponding to NH peak, and peaks at 1,720 and 1,680 cm^{-1}, corresponding to C=O groups. The ^{1}H NMR spectrum revealed the presence of a single signal at 5.36 ppm, which corresponded to olefinic proton, and the presence of two exchangeable singlet signals, corresponding to NH protons at 11.05 and 12.01 ppm, respectively. The ^{13}C NMR spectrum of compound **2** showed the presence of olefinic carbon at 74.73 ppm and carbonyl carbons of quinazolone and pyrazolone rings at 154.63 and 166.02 ppm, respectively. The cyclization was confirmed by HMBC experiment (Figure 2), where there were correlations between hydrogen at position 3 (5.36 ppm) with C-2 (166.02 ppm), C-3a (143.54 ppm), and C-9 (154.63 ppm), respectively. Finally, the mass spectrum showed its molecular ion peak *m/z* (M^+−1) at 199.9. All these findings confirmed the cyclization and formation of compound **2**.

The key intermediate pyrazolo[5,1-*b*]quinazoline-2,9(1*H*,4*H*)-dione **2** was used for the design of 3-arylidenepyrazolo[5,1-*b*]quinazoline-2,9(1*H*,3*H*)-dione **3a–j**, as a new scaffold targeting COX-2/5-LOX inhibitors.

Compounds **3a–j** were obtained by heating under reflux a solution of compound **2** in acetic acid, buffered with sodium acetate with an appropriate aromatic aldehyde. This reaction is proposed to proceed via the Knoevenagel reaction.[34,35] The structure of the prepared compounds **3a–j** was deduced from spectral data and microanalyses. The ^{1}H NMR spectra of these compounds characteristically revealed the disappearance of the signal of an olefinic proton at 5.36 ppm and the appearance of one singlet signal corresponding to C=CH of benzylidene in the range of δ: 5.47–5.69 ppm, in addition to an increase in the number of aromatic protons at δ: 6.74–8.10 ppm. The ^{13}C NMR spectra of compounds **3a–j** were used to confirm the structure of the new derivatives, which showed the disappearance of olefinic carbon at δ 74.73 ppm and the appearance of methylidene carbons in the range of δ: 88.13–89.88 ppm, in addition to the signals of aromatic carbons. The spectrum of compound

3d showed a triplet signal at δ: 7.08 ppm and a doublet of doublet signal at δ: 7.33 ppm, assigned to H-3′, 5′ and H-2′, 6′ protons of the *p*-fluoro-substituted benzylidene moiety, respectively. This is explained by proton coupling with fluorine atom.[36] The IR spectra of compounds **3e**, **3f**, **3h**, and **3j** showed the appearance of the band corresponding to aliphatic CH stretching in the range of 2,835–2,839 cm^{-1}. Moreover, the ^1H NMR spectra for these compounds revealed the presence of singlet signals in the region of 3.61–3.69 ppm, attributed to the OCH_3 protons, and the ^{13}C NMR spectra of the same compounds displayed an aliphatic signal of OCH_3 carbons in the region of 55.42–60.42 ppm.

2.2 | Biological evaluation

2.2.1 | In vitro COX-1 and COX-2 enzyme inhibition assays

All the newly synthesized compounds, **2** and **3a–j**, were evaluated for in vitro COX-1/COX-2 inhibition assays. The activities of synthesized compounds were measured as concentration causing 50% enzyme activity inhibition (IC_{50}; Table 1 and Figure 3). In addition, COX-2 selectivity indexes (SI values) were calculated as IC_{50} (COX-1)/IC_{50} (COX-2) and compared with celecoxib as a reference drug.

The in vitro assays revealed that many of the synthesized compounds showed a marked potency toward COX-1, as compounds **3a**, **3c**, **3d**, **3e**, and **3g** showed a comparable inhibitory activity (IC_{50} = 40.5, 127.2, 183, 111.6, and 165.77 nM, respectively) against celecoxib (IC_{50} = 187.88 nM). Compound **3a** potently inhibited COX-1, which might be attributed to the fact that **3a** was unsubstituted, thus possessing a potent activity to fit inside the COX-1 active site, due to its smaller pocket than that of COX-2. Therefore, compound **3a** showed the highest inhibitory activity toward COX-1 (IC_{50} = 40.5 nM) and the least selectivity toward COX-2 (SI = 0.19), which was unfavorable to the activity. In contrast, compound **3j** exhibited highest COX-2 inhibition (47 nM), superior to that of celecoxib (95.02 nM). In particular, compounds **3f**, **3h**, and **3j** showed clear preferential COX-2 over COX-1 inhibition, with remarkable SIs (3.04, 2.41, and 14.2, respectively), which were 7.17- to 1.21-fold higher than celecoxib (1.98).

The structure–activity relationship analysis revealed that methoxy-containing derivatives caused more potent inhibition of COX-2,[37] as the substitution pattern at position 3′, 4′, and 5′ of phenyl moiety with an electron-donating group like methoxy group of

TABLE 1 In vitro COX-1/COX-2 enzyme inhibition results and their selectivity index (SI)

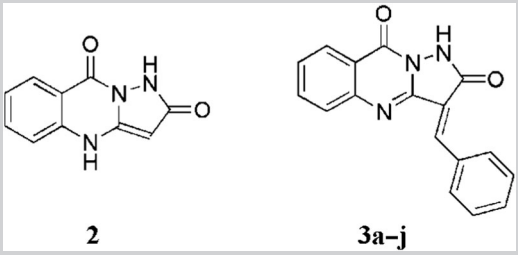

Compound no.	COX-1, IC_{50} (nM)[a]	COX-2, IC_{50} (nM)[a]	SI[b]
Celecoxib	187.8 ± 13.2	95.02 ± 3.8	1.98
2	218.0 ± 9.2	248 ± 8.6	0.88
3a	40.5 ± 2.1	215 ± 7.5	0.19
3b	472.7 ± 16.5	340.2 ± 11.5	1.39
3c	127.2 ± 7.4	308.6 ± 14.2	0.41
3d	183 ± 7.71	412 ± 18.9	0.44
3e	111.5 ± 5.2	259.8 ± 9.5	0.43
3f	1,485 ± 34.8	488.2 ± 21.2	**3.04**
3g	165.7 ± 6.3	345.7 ± 13.8	0.48
3h	684.1 ± 3.9	284.3 ± 16.1	**2.41**
3i	455 ± 15.8	326 ± 11.0	1.39
3j	667.6 ± 21.2	**47** ± 2.7	**14.2**

Note: The bold values reveal that they are more selective against COX-2.

[a]The IC_{50} value is the concentration required to produce 50% inhibition of COX-1, COX-2, or 5-LOX for means of three determinations ± standard deviation.

[b]In vitro COX-2 SI = IC_{50} of COX-1/COX-2.

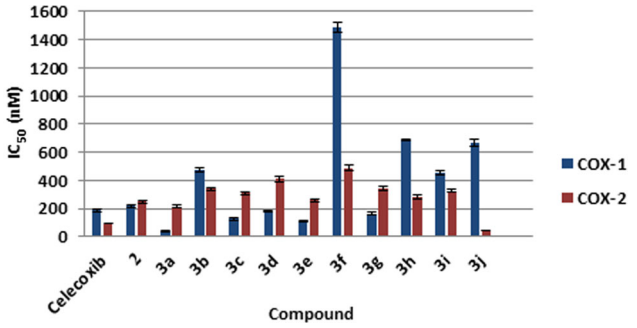

FIGURE 3 In vitro COX-1 and COX-2 enzyme inhibition assays of the synthesized compounds

the newly synthesized quinazolinone was a crucial element for the COX-2 inhibition and selectivity. Compound **3j** with trimethoxy groups greatly improved both COX-2 IC_{50} and selectivity, and afforded the most prominent compound (7.17-fold more selective than celecoxib), compared with the corresponding dimethoxy derivative **3h**, which was 1.21-fold more selective than celecoxib, and *para*-methoxy derivative **3f**, which was 1.54-fold more selective than celecoxib. This observation was consistent with the previously published work reporting that substitution with trimethoxy groups increased the anti-inflammatory activity.[29] In contrast, electron-withdrawing groups at the same positions resulted in a marked decrease in COX-2 inhibition and selectivity. Incorporation of 3-fluorophenyl moiety **3c**, 4-fluorophenyl moiety **3d**, and 4-chlorophenyl moiety **3g** showed a low inhibitory activity and selectivity against COX-2 enzyme.

Regarding *para* position of phenyl moiety, it is noteworthy that compounds having 4-methoxy substitution showed marked COX-2 selective inhibition (**3f**, **3h**, and **3j**). The increase in size due to the presence of methoxy group helped fitting the molecule into the larger pocket of COX-2 active site, in contrast with unsubstituted phenyl derivative **3a**, which showed the highest IC_{50} (40.51 nM) toward COX-1, superior to that of the reference drug celecoxib (IC_{50} = 187.88 nM) due to the smaller pocket of COX-1.

2.2.2 | In vivo anti-inflammatory activity: Carrageenan-induced rat paw edema

To explore the anti-inflammatory activity of the most promising compounds in COX-1 and COX-2 inhibition assay, compounds **3f**, **3h**, and **3j** were further subjected to in vivo evaluation of their anti-inflammatory activity, using carrageenan-induced rat paw edema assay method reported by Winter et al.[38] The increase in the volume of rat paw and the ability of compounds to inhibit edema over a period of 4 hr were monitored (results displayed in Table 2). All the investigated compounds, **3f**, **3h**, and **3j**, induced inhibition of edema percentage in the range of 39–44%, with anti-inflammatory activity almost identical to that of the reference standard agents (celecoxib or indomethacin).

2.2.3 | Determination of gastric ulcerogenic activity

Destruction of the gastric mucosa is one of the most common adverse effects due to the chronic administration of NSAIDs. Therefore, the gastric ulcerogenic potential for compounds **3a**, **3f**, **3h**, and **3j** was estimated. Isolated rat stomachs showed no ulceration for compounds **3f**, **3h**, and **3j**, which correlated with their selective COX-2 inhibitory profile in vitro, implying their gastric safety profile, whereas compound **3a** showed a marked ulcer effect, which is correlated with the results of in vitro COX-1 and COX-2 enzyme inhibition assays (Table 3).

2.2.4 | Determination of rat serum PGE2

The determination of serum PGE2 is a crucial parameter to evaluate the anti-inflammatory properties of the newly synthesized compounds. Being a chief inflammatory mediator, the reduction of PGE2 production in serum might contribute to the overall activity of the compounds. The same active compounds in the previous assay, **3f**, **3h**, and **3j**, were subjected to evaluation of PGE2 in rat serum; the results

TABLE 2 In vivo carrageenan-induced rat paw edema assay for analyzing the increase in the rat paw volume and percentage of edema inhibition

	Time (hr)					% Edema inhibition				
Compound	**0**	**1**	**2**	**3**	**4**	**0**	**1**	**2**	**3**	**4**
Control	0.71 ± 0.04	1.03 ± 0.07	1.96 ± 0.12	2.57 ± 0.81	2.98 ± 0.17	–	–	–	–	–
3f	0.63 ± 0.07	0.92 ± 0.09	1.64 ± 0.08*	1.72 ± 0.07*	1.63 ± 0.09*	11	10	16	33	45
3h	0.73 ± 0.06	0.99 ± 0.08	1.72 ± 0.05*	1.87 ± 0.03*	1.66 ± 0.06*	–	3	12	27	44
3j	0.73 ± 0.08	1.05 ± 0.04	1.81 ± 0.03*	2.03 ± 0.08*	1.82 ± 0.05*	–	–	7	21	39
Celecoxib	0.66 ± 0.06	0.95 ± 0.08	1.69 ± 0.07*	1.81 ± 0.05*	1.68 ± 0.06*	7	7	13	30	44
Indomethacin	0.68 ± 0.05	0.95 ± 0.07	1.63 ± 0.02*	1.71 ± 0.05*	1.64 ± 0.06*	4	7	16	33	45

Note: Average increase in paw volume (ml) ± *SE*.
Abbreviation: *SE*, standard error of the mean.
*Significantly different from the control group ($p < .05$).

TABLE 3 The gastric ulcerative effect of tested compounds **3a**, **3f**, **3h**, and **3j**, compared with celecoxib and indomethacin, on male albino rats ($n = 6$)

Groups	Score	
	No. of gastric ulcers	Severity lesions
Control (1 ml saline)	0	0
3a	4	4
3f	0.01	0
3h	0	0
3j	0	0
Celecoxib	0	0
Indomethacin	5	5

showed that they had good inhibition in PGE2 production, **3f** (67%), **3h** (65%), and **3j** (55%), in comparison with celecoxib (62%) and indomethacin (65%), as shown in Table 4.

These results revealed that all three compounds were more effective than or almost as effective as celecoxib in reducing the production of PGE2. Interestingly, the most active compound in this assay, compound **3f**, with a percentage inhibition of 67%, was the same compound with an SI of 3.04 toward COX-2 enzyme inhibition. The second most active compound in this assay, compound **3h**, with percentage inhibition of 65%, showed an SI of 2.40 toward COX-2 enzyme. These results showed a good correlation between the selective activity on COX-2 enzyme and the reduction in serum PGE2 production as one of the main inflammatory mediators produced through COX-2 enzyme pathways.

2.2.5 | In vitro 5-LOX inhibition assay

To minimize the side effects of COX-2 inhibitors, all the newly synthesized compounds were evaluated in vitro for their 5-LOX enzyme inhibition activity. Zileuton ($IC_{50} = 0.8\ \mu M$) was taken as the control (results shown in Table 5). The synthesized compounds showed an inhibitory activity against 5-LOX, with IC_{50} values of 0.6–4.3 μM. The 5-LOX inhibition activity data for the most potent compounds **3f**, **3h**, and **3j** in the aforementioned protocol revealed a clear preference for potency with monosubstituted $-OCH_3$ derivative **3f** ($IC_{50} = 0.6\ \mu M$). Disubstituted **3h** ($IC_{50} = 1.0\ \mu M$) and trisubstituted $-OCH_3$ **3j** ($IC_{50} = 2.3\ \mu M$) showed less inhibition activity, as compared with monosubstituted **3f**. From these results, we may conclude that the increase in the number of electron-donating groups will produce a decrease in the LOX activity of the compounds. Hence, compound **3f** showed excellent dual inhibition of COX-2/5-LOX and high selectivity.

TABLE 4 Determination of rat serum PGE2

Compound	Mean serum, conc. (ng/ml)	Inhibition (%)
Control (pre-carrageenan)	0.15 ± 0.01	NA
Control 1 (post-carrageenan)	0.65 ± 0.02	NA
3f	0.21 ± 0.01*	**67**
3h	0.23 ± 0.01*	**65**
3j	0.29 ± 0.02*	55
Celecoxib	0.24 ± 0.03*	**62**
Indomethacin	0.22 ± 0.02*	**65**

Note: The bold values indicate the highest prostaglandin inhibition percentage.
*Significantly different from control 1 (post-carrageenan) at $p < .05$.

TABLE 5 In vitro 5-LOX enzyme activities of the synthesized compounds

Compound	5-LOX, IC_{50} (μM)
Zileuton	0.8 ± 0.03
2	4.3 ± 0.12
3a	1.6 ± 0.03
3b	1.6 ± 0.02
3c	3.6 ± 0.14
3d	1.7 ± 0.03
3e	2.7 ± 0.09
3f	**0.6** ± 0.02
3g	1.8 ± 0.04
3h	1.0 ± 0.03
3i	2.7 ± 0.09
3j	2.3 ± 0.13

Note: The bold value indicates the best inhibition of 5-LOX enzyme.

2.2.6 | Effect of the Ca^{2+} ionophore A23187 on isolated polymorphonuclear leukocytes (PMNL) from experimental rats

A23187 is a calcium ionophore, which is used for 5-LOX activation and leukotriene formation in neutrophils, and is considered to be the appropriate assay to evaluate cellular 5-LOX activity; therefore, the newly synthesized compounds were further examined to see whether such compounds could prevent cells from generating leukotriene B4 (LTB4), indicative of 5-LOX activity, after stimulation of rat PMNL with Ca^{2+} ionophore A23187.

The results showed that the tested compounds showed a similar activity as zileuton; however, compound **3f** was superior to zileuton, demonstrating that monosubstitution with a methoxy group at *p*-position effectively suppressed the production of LTB4 in A23187-stimulated cells (Table 6).

TABLE 6 Effect of the Ca^{2+} ionophore A23187 on isolated polymorphonuclear leukocytes (PMNL) from experimental rats

Rats groups	LT (pg/10^6 cells)
Control	445 ± 24.8
Zileuton	95 ± 18.4*
2	433 ± 27.5@
3a	166 ± 21.1*,@
3b	157 ± 18.2*,@
3c	368 ± 28.2*,@
3d	174 ± 19.7*,@
3e	277 ± 24.4*,@
3f	61 ± 14.6*
3g	184 ± 22.6*,@
3h	211 ± 19.2*,@
3i	302 ± 24.2*,@
3j	260 ± 26.1*,@

Abbreviation: *LT*, leukotriene.
*Significantly different from the control group.
@Significantly different from zileuton.

2.3 | Molecular docking studies

Computer-aided drug design (CADD) is the science of using computers to optimize commercially available drugs (lead compounds) to identify new ligands with potential biological activities against certain biological targets. CADD is based on quantum mechanics and molecular modeling techniques. The traditional method of discovering new drugs is a very hectic process that consumes substantial amounts of effort, money, and time.[39–41] Computer-aided programs help to narrow the infinite number of options for lead optimization. Therefore, only the drug compounds with promising activities will be synthesized.

In the current study, we designed a 3-benzylidenepyrazolo[5,1-*b*]quinazoline-2,9(1*H*,3*H*)-dione scaffold **3a** as a novel COX-2 inhibitor via molecular docking studies. Docking of SC-558 in the binding site of COX-2 (Protein Data Bank code: 1CX2) was performed to clarify the key structural features required in the design of novel candidates of this class. The docking affinity indicates the biological binding mode, offering a relevant basis for the development of new COX-2 inhibitors.

2.3.1 | Docking study of SC-558

SC-558 was prepared using the ligand preparation tool, which adds hydrogens, fixes bad valences, and generates 3D coordinates using a catalyst. Docking was performed using the CDOCKER protocol. The pose cluster radius was set to 0.5 Å, the top 10 hits were used, and other docking parameters were kept at their default values. The results were analyzed according to their −CDOCKER_interaction_energy values. The docking protocol itself was validated through the redocking of the co-crystallized structure of the reference ligand (SC-558). Then, the resulting

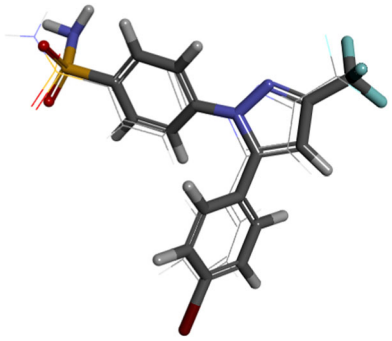

FIGURE 4 Alignment of the redocked conformer of SC-558 (stick) over the co-crystalized conformer (line) with a root mean square deviation value of 0.890

docking results/poses were compared with that of the crystallized reference ligand. This comparison was carried out by calculating the root mean square deviation (RMSD), and RMSD of 0.8900 was found, confirming the validity of the CDOCKER protocol (Figure 4).

The docking study of SC-558 showed a CDOCKER_interaction_energy of −48.42, and it forms seven hydrogen bonds: two hydrogen bonds between the F of the trifluoromethyl moiety and Arg120, three hydrogen bonds between the O of the sulfamoyl moiety and Arg513, and two hydrogen bonds of the NH of the sulfamoyl moiety with Ser353 and His90. Additionally, the planar regions of the pyrazole moiety form hydrophobic interactions with the hydrophobic pocket formed by amino acids Val349 and Ala527; the phenyl ring forms another van der Waals interaction with Ser353 and Val523; other phenyl ring forms hydrophobic interactions with Val523, Gly526, and Leu352; the *p*-bromo forms a hydrophobic interaction with Tyr385, Leu384, and Trp387. These interactions resembled the reported binding mode of SC-558 with cyclooxygenase (1CX2) but with additional hydrogen bonds (Figure 5).

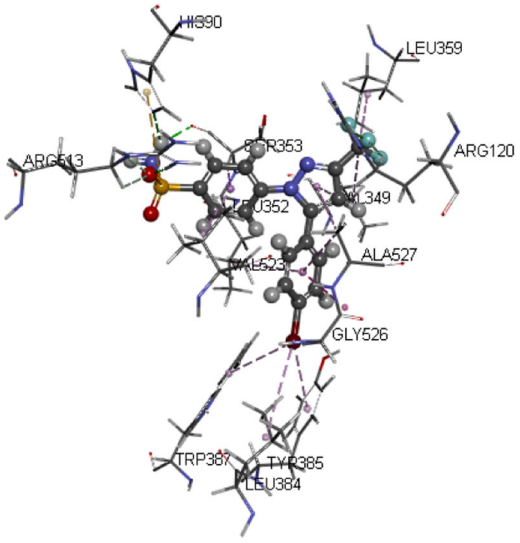

FIGURE 5 The three-dimensional image of the docking study of SC-558 reveals a CDOCKER_interaction_energy of −48.4274, with hydrogen and hydrophobic interactions in the COX-2 binding site (PDB code: 1CX2)

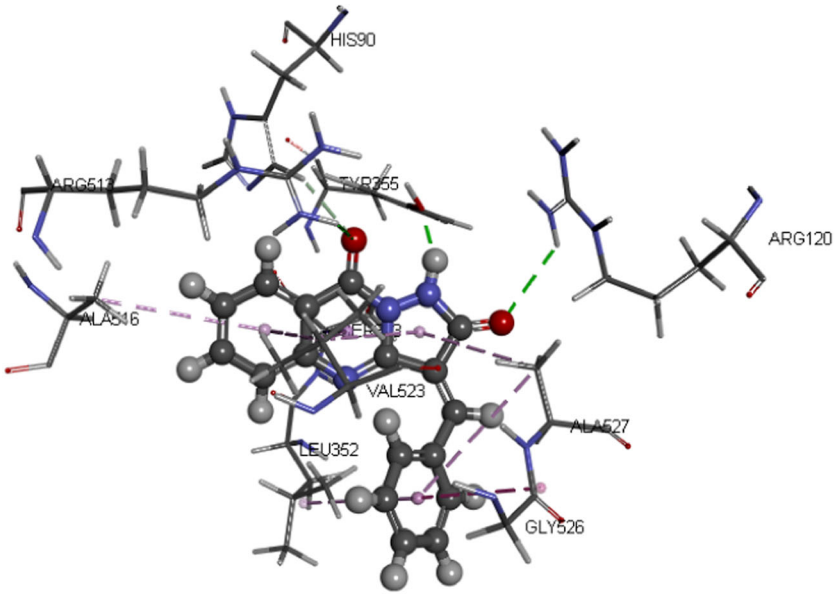

FIGURE 6 The three-dimensional image of the docking study of **3a** reveals a CDOCKER_interaction_energy of −30.46, with hydrogen and hydrophobic interactions in the COX-2 binding site (PDB code: 1CX2)

2.3.2 | The docking study of the new scaffold 3a

The docking study of 3-benzylidenepyrazolo[5,1-*b*]quinazoline-2,9(1*H*,3*H*)-dione **3a** showed a CDOCKER_interaction_energy of −30.46, and it forms four hydrogen bonds: one hydrogen bond between the O of 2-CO moiety and Arg120, two hydrogen bonds between the O of the 9-CO moiety and Arg513 and His90, and another hydrogen bond between the H of the NH of pyrazole moiety and Tyr355. Additionally, the planar regions of pyrazoloquinazoline moiety form hydrophobic interactions with the hydrophobic pocket formed by amino acids Ala527, Ser353, Val523, and Ala516, and another phenyl ring forms hydrophobic interactions with Ala527, Gly526, and Leu352 (Figure 6).

The docking study showed that the binding mode of compound **3a** inside COX-2 (1CX2) takes the same orientation geometry of the natural inhibitor SC-558, resulting in the design of 3-arylidenepyrazolo[5,1-*b*]quinazoline-2,9(1*H*,3*H*)-dione **3a–j** (Figure 7).

2.3.3 | Molecular docking of the compounds 3b–j into the COX-2 enzyme active site

With the aim of getting insights into the structural basis for compounds **3a–j**, we docked them into the binding site of the COX-2 enzyme, and docking studies revealed that they take the same geometric orientation of SC-558 in the binding site of COX-2 (Table 7 and Figure 8).

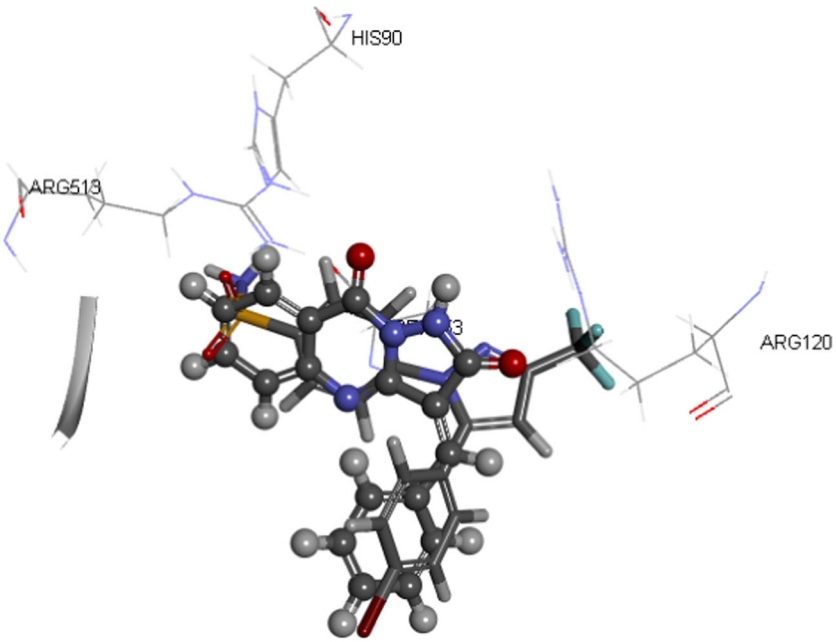

FIGURE 7 The three-dimensional image of the geometric orientation of the docked pose of the reference ligand SC-558 (stick) and the new scaffold (ball and stick) in the binding site of cyclooxygenase-2

TABLE 7 Docking score, hydrogen bonds, and hydrophobic interactions of compounds **3b–j** inside the COX-2 active site (PDB code: 1CX2)

Compound	−CDOCKER_interaction_energy	Binding interactions	Hydrogen bonds	Hydrophobic interactions
3b	31.63	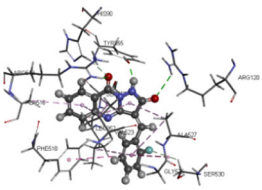	O of 2-CO with Arg120 O of 9-CO with Arg513 O of 9-CO with His90 H of NH with Tyr355 *o*-F with Ser530	Leu352, Phe518, Gly525, Ser530, Ala527 — phenyl pyrazolo, Val523 — pyrimidino benzo Ser353 with pyrimidine Ala527 with pyrazolo Ala516 with benzo
3c	31.08	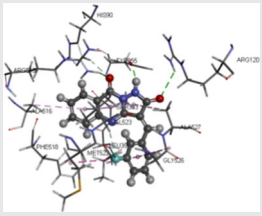	O of 2-CO with Arg120 O of 9-CO with Arg513 O of 9-CO with His90 H of NH with Tyr355 *m*-F with Ser530 *m*-F with Met522	Leu352, Phe518, Gly525, Ser530 — phenyl pyrazolo, Val523 — pyrimidino benzo Ser353 with pyrimidine Ala527 with pyrazolo Ala516 with benzo
3d	32.48	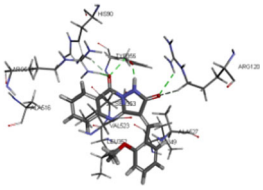	O of 2-CO with Arg120 O of 9-CO with Arg513 O of 9-CO with His90 H of NH with Tyr355	Leu352, Phe518, Gly525, Ser530, Ala527 — phenyl pyrazolo, Val523 — pyrimidino benzo Ser353 with pyrimidine Ala527 with pyrazolo Ala516 with benzo
3e	28.33	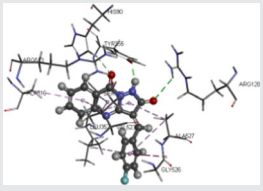	O of 2-CO with Arg120*2 O of 9-CO with Arg513 O of 9-CO with His90 O of 9-CO with Tyr355 H of NH with Tyr355	Leu352, Val349 — phenyl pyrazolo, Val523 — pyrimidino benzo Ser353 with pyrimidine Ala527 with pyrazolo Ala516 with benzo
3f	41.40	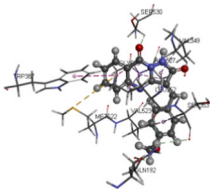	O of 9-CO with Ser530 O of methoxy with Ser353 O of methoxy with Leu352 H of methoxy with Gln192	Val523, Ser530 — phenyl Gly526, benzo — pyrimidino Ala527, pyrazolo — pyrimidine Trp387 with benzo
3g	32.64	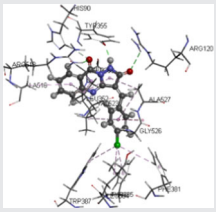	O of 2-CO with Arg120 O of 9-CO with Arg513 O of 9-CO with His90 H of NH with Tyr355	Leu352, Phe518, Gly525, Ser530, Ala527 — phenyl pyrazolo, Val523 — pyrimidino benzo Ser353 with pyrimidine Ala527 with pyrazolo Ala516 with benzo Phe381, Tyr385, Trp387 with chloro

(Continues)

TABLE 7 (Continued)

Compound	−CDOCKER_interaction_energy	Binding interactions	Hydrogen bonds	Hydrophobic interactions
3h	37.99	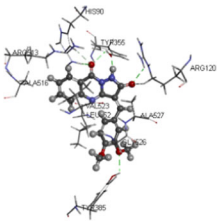	O of 2-CO with Arg120*2 O of 9-CO with Arg513 O of 9-CO with His90 H of NH with Tyr355 O of methoxy with Tyr385	Leu352, Phe518, Gly525, Ser530, Ala527 (phenyl) pyrazolo, Val523, benzo (pyrimidino) Ser353 with pyrimidine Ala527 with pyrazolo Ala516 with benzo
3i	30.08	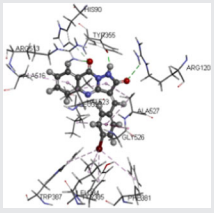	O of 2-CO with Arg120 O of 9-CO with Arg513 O of 9-CO with His90 H of NH with Tyr355	Leu352, Phe518, Gly525, Ser530, Ala527 (phenyl) pyrazolo, Val523, benzo (pyrimidino) Ser353 with pyrimidine Ala527 with pyrazolo Ala516 with benzo Leu384, Phe381, Tyr385, Trp387 with bromo
3j	45.08	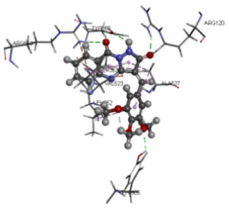	O of 2-CO with Arg120*3 O of 9-CO with Arg513 H of NH with Tyr355 O of methoxy with Tyr385	Leu352, Ala527 (phenyl) pyrazolo, Val523, benzo (pyrimidino) pyrimidine Ala527 (pyrazolo) Arg513 with benzo

The docking study of **3b–j** showed a CDOCKER_interaction_energy ranging from −28.33 to −45.08 (SC-558 has a score of −48.42), and most of the docked compounds form four hydrogen bonds: one hydrogen bond between the O of 2-CO moiety and Arg120, two hydrogen bonds between the O of the 9-CO moiety and Arg513 and His90, and another hydrogen bond between the H of the NH of pyrazole moiety and Tyr355. Additionally, the planar regions of pyrazoloquinazoline moiety form hydrophobic interactions with the hydrophobic pocket formed by amino acids Ala527, Ser353, Val523, and Ala516, and another phenyl ring forms hydrophobic interactions with Ala527 and Leu352, with an extra hydrogen bond with substituents such as *o*-fluoro, *m*-fluoro, *o*-methoxy, *m*-methoxy, *p*-methoxy, and *p*-bromo, as shown in Table 7. Compound **3j** has the highest docking score of the synthesized docked compounds of −45.08, revealing highest affinity to COX-2, and it forms five hydrogen bonds: three hydrogen bonds between the O of 2-CO moiety and Arg120, one hydrogen bond between the O of the 9-CO moiety and Arg513, and another hydrogen bond between the H of the NH of pyrazole moiety and Tyr355. Additionally, the planar regions of pyrazoloquinazoline moiety form hydrophobic interactions with the hydrophobic pocket formed by amino acids Ala527, Val523, and Arg513, and the phenyl ring forms hydrophobic interactions with Ala527 and Leu352, and forms an extra hydrogen bond with the *m*-methoxy group with Tyr385 (Figure 8).

2.3.4 | Molecular docking studies of 3f, 3h, and 3j in the 5-LOX enzyme active site (PDB: 3O8Y)

In this study, the molecular docking of the most active compounds, **3f**, **3h**, and **3j**, with the 5-LOX enzyme active site (PDB ID: 3O8Y) was carried out to predict and estimate the preferred binding mode. The predicted binding site of 5-LOX enzyme has been reported,[42] which

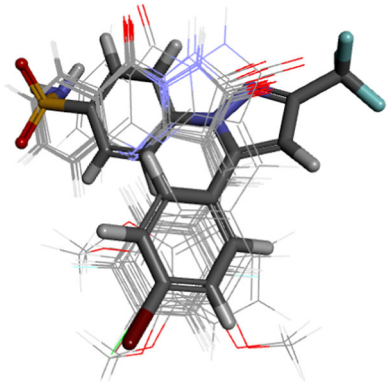

FIGURE 8 Alignment of docking poses of compounds **3a–j** (line), with SC-558 (stick) in the binding site of cyclooxygenase-2

includes the amino acid residues involved in the binding interaction. The catalytic center of 5-LOX mainly consists of the amino acid residues Leu368, Ile406, Ala410, Leu414, Ile415, Leu691, Val604, and Leu607, which have a hydrophobic character. The iron atom is located in the middle of the active site and is stabilized by forming coordination bonds with His367, His372, His550, and Asn554. The results of the docking study are reported as binding free energy (Δ*G*).

Zileuton belongs to the group of chelating inhibitors of the 5-LOX, chelating the active iron (Fe) site of the enzyme.[43] The proposed binding mode of reference ligand, zileuton (IC_{50} = 0.8 μM), showed an affinity value of −80.03 kcal/mol. In zileuton, the carbonyl group of urea moiety is involved in a hydrogen bonding interaction with Asn425, the amino group is stabilized by a hydrophilic interaction with His600, and the hydroxyl group is involved in a hydrogen bonding interaction with Gln363. In addition, the ethyl group is located in the hydrophobic pocket formed by Leu414, Leu420, and Phe421. In contrast, benzothiophene moiety of the zileuton is located in lipophobic interactions with the hydrophobic part of Gln363, Leu368, Ala410, Ile415, and Leu607. Furthermore, benzothiophene moiety is stabilized by anion–π interaction with key residue, Tyr181, and aromatic stacking interactions with Phe177, His367, and His372, which increase the interaction between three conserved histidine amino acid groups and iron, as well as the main-chain carboxylate of the C-terminus, Ile673 (Figure 9).

The obtained binding mode for compound **3f**, which showed an affinity value of −90.63 kcal/mol, suggested that the oxygen atom of methoxy group moiety is involved in a hydrogen bonding interaction with His360 and the amino group of pyrazole moiety and carbonyl group of quinazoline moiety are stabilized by hydrogen bonding interaction with Tyr181, which is involved in an aromatic stacking interaction with the key residue, Trp599. Also, the methyl group is involved in hydrophobic interactions with Ala426, Pro569, His360, and His600. Moreover, the phenyl ring of compound **3f** is involved in hydrophobic interactions with Thr364, Ala603, and Val604, and it is

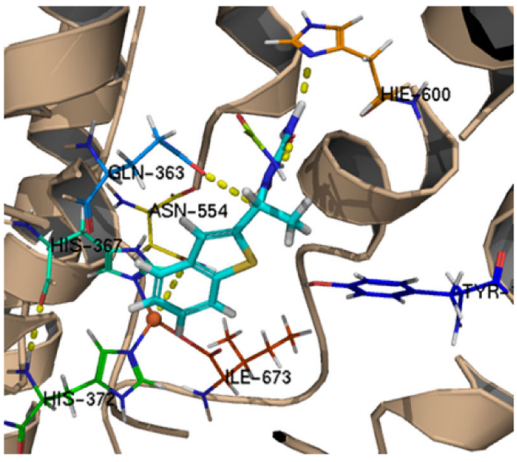

FIGURE 9 The predicted binding mode of zileuton at the binding site of 5-LOX (PDB: 3O8Y). H-bonds (yellow dotted lines), hydrogen (white), nitrogen (blue), oxygen (red), and sulfur (yellow). Iron atom is shown in orange color

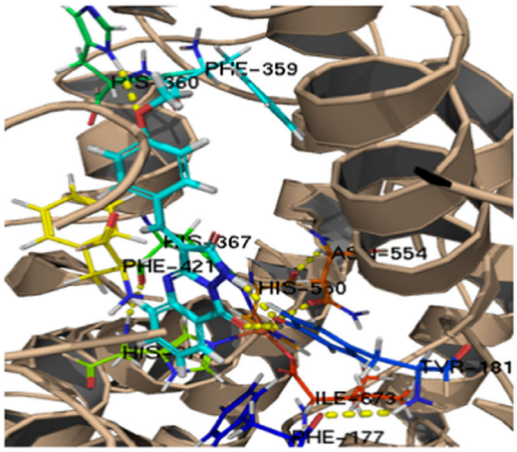

FIGURE 10 The predicted binding mode of **3f** at the binding site of 5-LOX (PDB: 3O8Y). H-bonds (yellow dotted lines), hydrogen (white), nitrogen (blue), oxygen (red), and sulfur (yellow). Iron atom is shown in orange color

stabilized by aromatic stacking interactions with Phe359, His432, and Phe421.

Quinazoline moiety is located in the hydrophobic pocket formed by Leu368, Ile406, Leu607, Ala410, Leu414, Ile415, and Ala603, and it forms an aromatic stacking network with Phe177, His367, His372, and His550, a pocket that contributes to increase in the affinity of compound **3f**. The most active compound, **3f**, is involved in interactions with Tyr181, Thr364, His600, Ala603, and Ala606, which are specific to 5-LOX enzyme and could be responsible for selectivity (Figure 10).

The binding mode of compounds **3h** and **3j** is similar to that of compound **3f**, with affinity values of −80.59 and −70.50 kcal/mol, respectively. Compounds **3h** and **3j** have the same hydrophilic and hydrophobic interactions. However, the insertion of another methoxy group in compound **3h** decreases the strength of hydrophilic interactions; therefore, it is expected to be much less potent than compound **3f**. Additionally, the insertion of two methoxy groups in compound **3j** results in unfavorable interactions due to steric effects induced by three methoxy groups, which explain the lower affinity of compound **3j**, compared with compound **3f** (Figure 11).

In conclusion, the molecular docking study results with 5-LOX enzyme indicated that the reference drug and synthesized compounds have similar binding mode patterns; also, our study has confirmed that most of the synthesized compounds have good binding affinities toward the receptor target and the computed values of free energy of binding of the synthesized compounds reflect the overall trend (Table 8).

3 | CONCLUSION

The current study proposed a rational design of new anti-inflammatory compounds **3a–j**. The design is based on the

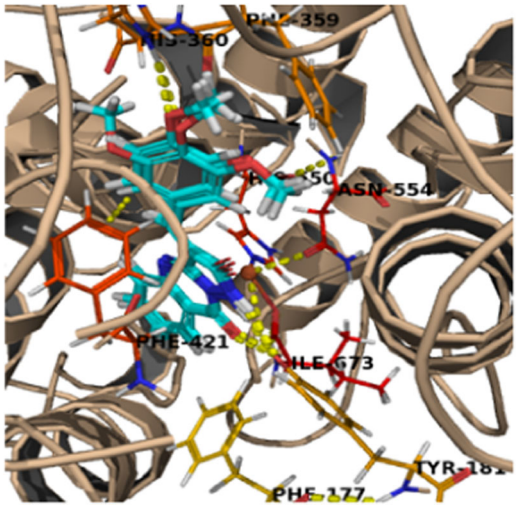

FIGURE 11 Alignment of compounds **3f**, **3h**, and **3j** at the binding site of 5-LOX (PDB: 3O8Y). H-bonds (yellow dotted lines), hydrogen (white), nitrogen (blue), oxygen (red), and sulfur (yellow)

hybridization of pharmacophores having different anti-inflammatory actions, with the aim of finding new candidates with anti-inflammatory activity by inhibiting both COX-2 and 5-LOX enzymes, overcoming the side effects of other selective COX-2 inhibitors. In light of the pharmacological activity, promising anti-inflammatory activities, compared with reference drug, celecoxib, were observed with compounds **3f**, **3h**, and **3j** that exhibited SIs of 3.04, 2.4, and 14.2, respectively, which were 1.22- to 7.21-fold higher than that of celecoxib (SI = 1.98). The three most active compounds, **3f**, **3h**, and **3j**, were further screened in vivo, showing remarkable results, in comparison with celecoxib, as anti-inflammatory agents, where they exhibited inhibition of percentage edema in the range of 39–45%, which is a marked anti-inflammatory activity in comparison to both celecoxib (44%) and indomethacin (45%). Moreover, the same candidates were screened for ulcerogenic adverse effects. The results revealed that none of these compounds showed a gastric ulcerogenic effect. They showed similar manners of interaction to that of SC-558 and zileuton. Interestingly, these derivatives also decreased the production of PGE2, with the percentage inhibition ranging from 55% to 67%, where the most active compound in PGE2 assay, **3f**, with percentage inhibition of 67%, is the same compound with an SI of 3.04 toward COX-2 enzyme and 5-LOX inhibitory activity with an IC_{50} value of 0.6 μM, which was better than zileuton (IC_{50} = 0.8 μM). Taken together, these observations suggest that 3-(4-methoxybenzylidene) pyrazolo[5,1-*b*]quinazoline-2,9(1*H*,3*H*)-dione (**3f**) represents a new scaffold to design potent, effective, and safe anti-inflammatory agents possessing a dual COX-2/5-LOX inhibitory activity, encouraging further future investigation for these derivatives, as they act on enzymes involved in both arachidonic acid pathways.

4 | EXPERIMENTAL

4.1 | Chemistry

4.1.1 | General

Melting points were determined on the Stuart apparatus and the values given were uncorrected. The IR spectra were determined on Shimadzu IR 435 spectrophotometer (Shimadzu Corp., Kyoto, Japan), Microanalytical Center, Faculty of Pharmacy, Cairo University, and values were represented in cm^{-1}. The ^{1}H NMR spectra were recorded using a Bruker 400 MHz (Bruker Corp., Billerica, MA) spectrophotometer, Microanalytical Center, Faculty of Pharmacy, Cairo University, Egypt. Tetramethylsilane was used as the internal standard, chemical shift values were recorded in parts per million on δ scale, and coupling constants (J) were given in hertz. The ^{13}C NMR spectra were carried out using Bruker 100-MHz spectrophotometer, Microanalytical Center, Faculty of Pharmacy, Cairo University, Egypt. Microanalyses for C, H, and N were carried out at the Regional Center for Mycology and Biotechnology, Faculty of Pharmacy, Al Azhar University, Egypt. The progress of the reactions was monitored using thin-layer chromatography aluminum sheets precoated with UV fluorescent silica gel Merck 60 F254. The spots were visualized using a UV lamp.

The NMR spectra as well as the InChI codes of the investigated compounds, together with some biological activity data, are provided as Supporting Information Data.

The preparation of 3-amino-*1H*-5(*4H*)-one (**1**) was performed according to reported procedures.[33]

*Pyrazolo[5,1-b]quinazoline-2,9(1H,4H)-dione (**2**)*

Anthranilic acid (13.7 g, 0.1 mol) and 3-amino-1*H*-5(*4H*)-one (**1**) (9.9 g, 0.1 mol) were added to a solution of concentrated hydrochloric acid (10 ml) in water (30 ml). The reaction mixture was

TABLE 8 Docking score, hydrogen bonds, and aromatic stacking interactions of compounds **3f**, **3h**, and **3j** inside the 5-LOX active site (PDB code: 3O8Y)

Compound no.	Δ*G* (kcal/mol)	No. of hydrogen bonding interactions	No. of aromatic stacking interactions
Zileuton	−80.03	Gln363, Asn425, and His600	Phe177, Tyr181, His367, and His372
3f	−90.63	Tyr181 and His360	Phe177, Tyr181, Phe359, His367, His372, Phe421, and His432
3h	−80.59	Tyr181 and His360	Phe177, Tyr181, Phe359, His367, His372, and Phe421
3j	−70.50	Tyr181 and Thr427	Phe177, Tyr181, Phe359, His367, His372, and Phe421

heated under reflux for 3 hr and cooled, and the separated solid was filtered, washed with water, dried, and crystallized from ethanol. Yield: 55%; m.p.: >300°C; IR (KBr) cm^{-1}: 3,201 (NH), 3,082 (arom. CH), 1,720, 1,680 (C=O); ^1H NMR (dimethyl sulfoxide [DMSO]-d_6, D_2O) δ ppm: 5.36 (s, 1H, olefinic CH), 7.19 (t, J = 7.84 Hz, 1H, arom. CH), 7.30 (d, J = 8.24 Hz, 1H, arom. CH), 7.66 (t, J = 7.72 Hz, 1H, arom. CH), 8.09 (d, J = 8.00 Hz, 1H, arom. CH), 11.05 (s, brd, 1H, NH, D_2O exchangeable), 12.01 (s, 1H, NH, D_2O exchangeable); ^{13}C NMR (DMSO-d_6) δ ppm: 74.73 (C3, pyrazoloquinazoline), 112.58 (C8a, pyrazoloquinazoline), 116.08 (C5, pyrazoloquinazoline), 121.67 (C7, pyrazoloquinazoline), 127.64 (C8, pyrazoloquinazoline), 134.50 (C6, pyrazoloquinazoline), 139.64 (C4a, pyrazoloquinazoline), 143.54 (C3a, pyrazoloquinazoline), 154.63 (C9, pyrazoloquinazoline, C=O), 166.02 (C2, pyrazoloquinazoline, C=O); MS m/z (% rel. abundance): 200 (M−1, 100%), 190 (13%); anal. calcd. for $C_{10}H_7N_3O_2$ (201.18): C, 59.70; H, 3.48; N, 20.89; found C, 59.93; H, 3.64; N, 21.11.

4.1.2 | General procedure for the synthesis of compounds 3a–j

The appropriate aromatic aldehyde (0.001 mol) was added to a solution of pyrazolo[5,1-*b*]quinazoline-2,9(1*H*,4*H*)-dione (**2**) (0.2 g, 0.001 mol) in acetic acid (10 ml) buffered with sodium acetate (0.08 g, 0.001 mol). The mixture was refluxed for 5 hr, cooled, and then poured into water. The precipitate was filtered, washed with water, and crystallized from ethanol.

*(3Z)-3-Benzylidenepyrazolo[5,1-*b*]quinazoline-2,9(1*H*,3*H*)dione (**3a**)*

Yield: 82%; m.p.: >300°C; IR (KBr) cm^{-1}: 3,367 (NH), 3,116 (arom. CH), 1,701, 1,689 (C=O), 1,604 (C=N); ^1H NMR (DMSO-d_6, D_2O) δ ppm: 5.55 (s, 1H, C=CH), 7.15 (t, J = 7 Hz, 1H, arom. CH), 7.24–7.32 (m, 5H, arom. CH), 7.37 (d, J = 8.08 Hz, 1H, arom. CH), 7.71 (t, J = 7.74 Hz, 1H, arom. CH), 8.08 (d, J = 7.54 Hz, 1H, arom. CH), 12.70 (s, 1H, NH, D_2O exchangeable); ^{13}C NMR (DMSO-d_6) δ ppm: 89.52 (C3, pyrazoloquinazoline), 113.00 (C8a, pyrazoloquinazoline), 116.49 (C5, pyrazoloquinazoline), 122.34 (C7, pyrazoloquinazoline), 126.59 (C4, benzene), 127.41 (C8, pyrazoloquinazoline), 127.59 (C2, C6, benzene), 128.67 (C3, C5, benzene), 134.92 (C1, benzene), 139.80 (methylidene carbon, C6, pyrazoloquinazoline), 141.97 (C4a, pyrazoloquinazoline), 142.54 (C3a, pyrazoloquinazoline), 153.12 (C9, pyrazoloquinazoline, C=O), 166.29 (C2, pyrazoloquinazoline, C=O); anal. calcd. for $C_{17}H_{11}N_3O_2$ (289.29): C, 70.58; H, 3.80; N, 14.53; found C, 70.46; H, 3.91; N, 14.69.

*(3Z)-3-(2-Fluorobenzylidene)pyrazolo[5,1-*b*]quinazoline-2,9(1*H*,3*H*)-dione (**3b**)*

Yield: 80%; m.p.: 263–265°C; IR (KBr) cm^{-1}: 3,228 (NH), 3,078 (arom. CH), 1,708, 1,651 (C=O), 1,585 (C=N); ^1H NMR (DMSO-d_6, D_2O) δ ppm: 5.69 (s, 1H, C=CH), 7.07 (t, J = 8.2 Hz, 1H, arom. CH), 7.25 (dt, J = 12.5, 6.8 Hz, 3H, arom. CH), 7.37 (dd, J = 18.3, 8.2 Hz, 2H, arom. CH), 7.73 (t, J = 7.6 Hz, 1H, arom. CH), 8.08 (d, J = 7.8 Hz, 1H, arom. CH), 12.75 (s, 1H, NH, D_2O exchangeable); ^{13}C NMR (DMSO-d_6) δ ppm: 88.13 (C3, pyrazoloquinazoline), 112.91 (C8a, pyrazoloquinazoline), 115.54 (d, J = 20 Hz, C3, benzene), 116.48 (C5, pyrazoloquinazoline), 122.50 (C1, benzene), 124.42 (C5, benzene), 127.42 (C7, pyrazoloquinazoline), 128.67 (C8, pyrazoloquinazoline), 128.86 (d, J = 6.0 Hz, C4, benzene), 129.90 (d, J = 3.0 Hz, C6, benzene), 135.03 (C6, pyrazoloquinazoline), 139.75 (methylidene carbon, C4a, pyrazoloquinazoline), 142.66 (C3a, pyrazoloquinazoline), 153.10 (C9, pyrazoloquinazoline, C=O), 159.35 (d, J = 244 Hz, C2, benzene), 166.12 (C2, pyrazoloquinazoline, C=O); anal. calcd. for $C_{17}H_{10}FN_3O_2$ (307.28): C, 66.45; H, 3.25; N, 13.68; found C, 66.21; H, 3.49; N, 13.85.

*(3Z)-3-(3-Fluorobenzylidene)pyrazolo[5,1-*b*]quinazoline-2,9(1*H*,3*H*)-dione (**3c**)*

Yield: 78%; m.p.: >300 °C; IR (KBr) cm^{-1}: 3,290 (NH), 3,059 (arom. CH), 1,718, 1,712 (C=O), 1,612 (C=N); ^1H NMR (DMSO-d_6, D_2O) δ ppm: 5.56 (s, 1H, C=CH), 6.99 (t, J = 8.1 Hz, 1H, arom. CH), 7.11–7.14 (m, 2H, arom. CH), 7.24 (dt, J = 14.9, 7.2 Hz, 2H, arom. CH), 7.37 (d, J = 8.3 Hz, 1H, arom. CH), 7.71 (t, J = 8.0 Hz, 1H, arom. CH), 8.08 (d, J = 8.0 Hz, 1H, arom. CH), 12.68 (s, 1H, NH, D_2O exchangeable); ^{13}C NMR (DMSO-d_6) δ ppm: 89.02 (C3, pyrazoloquinazoline), 113.08 (C8a, pyrazoloquinazoline), 113.36 (d, J = 21 Hz, C2, benzene), 114.34 (d, J = 22 Hz, C4, benzene), 116.48 (C5, pyrazoloquinazoline), 122.41 (C7, pyrazoloquinazoline), 123.68 (C6, benzene), 127.38 (C8, pyrazoloquinazoline), 130.47 (d, J = 9.0 Hz, C5, benzene), 134.92 (C6, pyrazoloquinazoline), 139.76 (C1, benzene, CH, methylidene carbon), 142.69 (C4a, pyrazoloquinazoline), 145.07 (C3a, pyrazoloquinazoline), 153.10 (C9, pyrazoloquinazoline, C=O), 161.60 (d, J = 241 Hz, C3, benzene), 166.25 (C2, pyrazoloquinazoline, C=O); anal. calcd. for $C_{17}H_{10}FN_3O_2$ (307.28): C, 66.45; H, 3.25; N, 13.68; found C, 66.34; H, 3.46; N, 13.90.

*(3Z)-3-(4-Fluorobenzylidene)pyrazolo[5,1-*b*]quinazoline-2,9(1*H*,3*H*)-dione (**3d**)*

Yield: 71%; m.p.: >300°C; IR (KBr) cm^{-1}: 3,186 (NH), 2,974 (arom. CH), 1,697, 1,654 (C=O), 1,604 (C=N); ^1H NMR (DMSO-d_6, D_2O) δ ppm: 5.55 (s, 1H, C=CH), 7.08 (t, J = 8.8 Hz, 2H, arom. CH), 7.25 (t, J = 7.5 Hz, 1H, arom. CH), 7.33 (dd, 2H, J = 8.2, 5.6 Hz, 2H, arom. CH), 7.37 (d, J = 8.0 Hz, 1H, arom. CH), 7.72 (t, J = 7.4 Hz, 1H, arom. CH), 8.07 (d, J = 7.7 Hz, 1H, arom. CH), 12.70 (s, 1H, NH, D_2O exchangeable); ^{13}C NMR (DMSO-d_6) δ ppm: 89.42 (C3, pyrazoloquinazoline), 113.03 (C8a, pyrazoloquinazoline), 115.40 (d, J = 21 Hz, C3, C5, benzene), 116.51 (C5, pyrazoloquinazoline), 122.34 (C7, pyrazoloquinazoline), 127.40 (C8, pyrazoloquinazoline), 129.53 (d, J = 8.0 Hz, C2, C6, benzene), 134.90 (C1, benzene), 138.10 (C6, pyrazoloquinazoline), 139.80 (CH, methylidene carbon, C4a, pyrazoloquinazoline), 142.48 (C3a, pyrazoloquinazoline), 153.14 (C9, pyrazoloquinazoline, C=O), 160.04 (d, J = 241 Hz, C4, benzene), 166.21 (C2, pyrazoloquinazoline, C=O); anal. calcd. for $C_{17}H_{10}FN_3O_2$ (307.28): C, 66.45; H, 3.25; N, 13.68; found C, 66.39; H, 3.37; N, 13.87.

*(3Z)-3-(2-Methoxybenzylidene)pyrazolo[5,1-b]quinazoline-2,9(1H,3H)-dione (**3e**)*

Yield: 85%; m.p.: 293–295°C; IR (KBr) cm^{-1}: 3,217 (NH), 3,074 (arom. CH), 2,835 (aliph. CH), 1,712, 1,701 (C=O), 1,615 (C=N); ^1H NMR (DMSO-d_6, D_2O) δ ppm: 3.64 (s, 3H, OCH_3), 5.60 (s, 1H, C=CH), 6.81 (t, J = 7.44 Hz, 1H, arom. CH), 6.89 (d, J = 8 Hz, 1H, arom. CH), 7.14 (t, J = 7.44 Hz, 1H, arom. CH), 7.24–7.28 (m, 2H, arom. CH), 7.50 (d, J = 8.28 Hz, 1H, arom. CH), 7.73 (t, J = 7.24 Hz, 1H, arom. CH), 8.08 (d, J = 7.64 Hz, 1H, arom. CH), 12.82 (s, 1H, NH, D_2O exchangeable); ^{13}C NMR (DMSO-d_6) δ ppm: 55.89 (OCH_3), 88.81 (C3, pyrazoloquinazoline), 111.27 (C3, benzene), 112.54 (C8a, pyrazoloquinazoline, C1, benzene), 116.33 (C5, pyrazoloquinazoline), 120.35 (C5, benzene), 122.83 (C7, pyrazoloquinazoline), 127.38 (C8, pyrazoloquinazoline), 128.18 (C6 benzene), 128.26 (C4 benzene), 129.19 (C6, pyrazoloquinazoline), 135.43 (CH, methylidene carbon), 139.60 (C4a, pyrazoloquinazoline), 143.18 (C3a, pyrazoloquinazoline), 153.09 (C2, benzene), 156.91 (C9, pyrazoloquinazoline, C=O), 166.47 (C2, pyrazoloquinazoline, C=O); anal. calcd. for $C_{18}H_{13}N_3O_3$ (319.31): C, 76.71; H, 4.07; N, 13.16; found C, 76.90; H, 4.33; N, 13.49.

*(3Z)-3-(4-Methoxybenzylidene)pyrazolo[5,1-b]quinazoline-2,9(1H,3H)-dione (**3f**)*

Yield: 73%; m.p.: 241–243°C; IR (KBr) cm^{-1}: 3,209 (NH), 3,062 (arom. CH), 2,835 (aliph. CH), 1,654, 1,680 (C=O), 1,597 (C=N); ^1H NMR (DMSO-d_6, D_2O) δ ppm: 3.69 (s, 3H, OCH_3), 5.49 (s, 1H, C=CH), 6.80 (d, J = 8.68 Hz, 2H, arom. CH), 7.19–7.27 (m, 3H, arom. CH), 7.37 (d, J = 7.68 Hz, 1H, arom. CH), 7.70 (t, J = 7.36 Hz, 1H, arom. CH), 8.07 (d, J = 7.88 Hz, 1H, Ar-H), 12.65 (s, 1H, NH, D_2O exchangeable); ^{13}C NMR (DMSO-d_6) δ ppm: 55.42 (OCH_3), 89.84 (C3, pyrazoloquinazoline), 112.97 (C8a, pyrazoloquinazoline), 114.00 (C3, C5, benzene), 116.51 (C5, pyrazoloquinazoline), 122.27 (C7, pyrazoloquinazoline), 127.40 (C8, pyrazoloquinazoline, C1 benzene), 128.60 (C2, C6, benzene), 133.78 (C6, pyrazoloquinazoline), 134.87 (methylidene carbon), 139.85 (C4a, pyrazoloquinazoline), 142.42 (C3a, pyrazoloquinazoline), 153.16 (C4, benzene), 158.08 (C9, pyrazoloquinazoline, C=O), 166.30 (C2, pyrazoloquinazoline, C=O); anal. calcd. for $C_{18}H_{13}N_3O_3$ (319.31): C, 76.71; H, 4.07; N, 13.16; found C, 76.94; H, 4.30; N, 13.42.

*(3Z)-3-(4-Chlorobenzylidene)pyrazolo[5,1-b]quinazoline-2,9(1H,3H)-dione (**3g**)*

Yield: 70%; m.p.: 280–282°C; IR (KBr) cm^{-1}: 3,363 (NH), 3,047 (arom. CH), 1,720, 1,680 (C=O), 1,597 (C=N); ^1H NMR (DMSO-d_6, D_2O) δ ppm: 5.55 (s, 1H, C=CH), 7.23 (t, J = 7.48 Hz, 1H, arom. CH), 7.28–7.33 (m, 4H, arom. CH), 7.36 (d, J = 8.24 Hz, 1H, arom. CH), 7.70 (t, J = 7.36 Hz, 1H, arom. CH), 8.07 (d, J = 7.92 Hz, 1H, arom. CH), 12.73 (s, 1H, NH, D_2O exchangeable); ^{13}C NMR (DMSO-d_6) δ ppm: 89.18 (C3, pyrazoloquinazoline), 113.01 (C8a, pyrazoloquinazoline), 116.65 (C5, pyrazoloquinazoline), 122.30 (C7, pyrazoloquinazoline), 127.37 (C8, pyrazoloquinazoline), 128.52 (C2, C6, benzene), 129.53 (C3, C5, benzene), 131.17 (C1, benzene), 134.87 (methylidene carbon, C6, pyrazoloquinazoline), 140.03 (C4, benzene), 141.07 (C4a, pyrazoloquinazoline), 142.74 (C3a, pyrazoloquinazoline), 153.25 (C9, pyrazoloquinazoline, C=O), 166.36 (C2, pyrazoloquinazoline, C=O); anal. calcd. for $C_{17}H_{10}ClN_3O_2$ (323.73): C, 63.06; H, 3.09; N, 12.98; found C, 63.29; H, 3.17; N, 12.78.

*(3Z)-3-(3,4-Dimethoxybenzylidene)pyrazolo[5,1-b]quinazoline-2,9(1H,3H)-dione (**3h**)*

Yield: 72%; m.p.: 250–252°C; IR (KBr) cm^{-1}: 3,221 (NH), 3,062 (arom. CH), 2,835 (aliph. CH), 1,718, 1,685 (C=O), 1,597 (C=N); ^1H NMR (DMSO-d_6, D_2O) δ ppm: 3.62 (s, 3H, OCH_3), 3.69 (s, 3H, OCH_3), 5.48 (s, 1H, C=CH), 6.84 (s, 2H, arom. CH), 6.94 (s, 1H, arom. CH), 7.23 (t, J = 7.48 Hz, 1H, arom. CH), 7.39 (d, J = 7.48 Hz, 1H, arom. CH), 7.71 (t, J = 7.2 Hz, 1H, arom. CH), 8.07 (d, J = 7.8 Hz, 1H, arom. CH), 12.76 (s, 1H, NH, D_2O exchangeable); ^{13}C NMR (DMSO-d_6) δ ppm: 55.93 (OCH_3), 56.07 (OCH_3), 89.88 (C3, pyrazoloquinazoline), 112.06 (C2, benzene), 112.12 (C8a, pyrazoloquinazoline), 112.96 (C5, benzene), 116.49 (C5, pyrazoloquinazoline), 119.70 (C6, benzene), 122.31 (C7, pyrazoloquinazoline), 127.40 (C8, pyrazoloquinazoline, C1, benzene), 134.45 (C6, pyrazoloquinazoline), 134.92 (methylidene carbon), 139.87 (C4a, pyrazoloquinazoline), 142.44 (C3a, pyrazoloquinazoline), 147.83 (C4, benzene), 148.92 (C3, benzene), 153.15 (C9, pyrazoloquinazoline, C=O), 166.32 (C2, pyrazoloquinazoline, C=O); anal. calcd. for $C_{19}H_{15}N_3O_4$ (349.34): C, 65.32; H, 4.29; N, 12.03; found C, 65.48; H, 4.46; N, 12.31.

*(3Z)-3-(4-Bromobenzylidene)pyrazolo[5,1-b]quinazoline-2,9(1H,3H)-dione (**3i**)*

Yield: 68%; m.p.: >300°C; IR (KBr) cm^{-1}: 3,170 (NH), 2,970 (arom. CH), 1,751, 1,724 (C=O), 1,597 (C=N); ^1H NMR (DMSO-d_6, D_2O) δ ppm: 5.52 (s, 1H, C=CH), 7.26 (t, J = 8.24 Hz, 2H, arom. CH), 7.37–7.45 (m, 2H, arom. CH), 7.73 (t, J = 7.28 Hz, 2H, arom. CH), 7.37 (d, J = 8.28 Hz, 1H, arom. CH), 8.08 (d, J = 7.84 Hz, 1H, arom. CH), 12.09 (s, 1H, NH, D_2O exchangeable); ^{13}C NMR (DMSO-d_6) δ ppm: 89.04 (C3, pyrazoloquinazoline), 113.05 (C8a, pyrazoloquinazoline), 116.51 (C5, pyrazoloquinazoline), 119.70 (C4, benzene), 122.39 (C7, pyrazoloquinazoline), 127.42 (C2, C6, benzene), 129.97 (C8, pyrazoloquinazoline), 131.49 (C3, C5, benzene), 134.93 (C6, pyrazoloquinazoline), 139.78 (C1, benzene), 141.48 (methylidene carbon), 142.52 (C4a, pyrazoloquinazoline), 153.16 (C3a, pyrazoloquinazoline), 166.14 (C9, pyrazoloquinazoline, C=O), 172.47 (C2, pyrazoloquinazoline, C=O); anal. calcd. for $C_{17}H_{10}BrN_3O_2$ (368.18): C, 55.43; H, 2.71; N, 11.41; found C, 55.61; H, 2.85; N, 11.70.

*(3Z)-3-(3,4,5-Trimethoxybenzylidene)pyrazolo[5,1-b]quinazoline-2,9(1H,3H)-dione (**3j**)*

Yield: 65%; m.p.: 253–255°C; IR (KBr) cm^{-1}: 3,226 (NH), 3,062 (arom. CH), 2,835 (aliph. CH), 1,697, 1,654 (C=O), 1,600 (C=N); ^1H NMR (DMSO-d_6, D_2O) δ ppm: 3.61 (s, 3H, OCH_3), 3.66 (s, 6H, $2OCH_3$), 5.47 (s, 1H, C=CH), 6.74 (s, 2H, arom. CH), 7.23 (t, J = 7.56 Hz, 1H, arom. CH), 7.41 (d, J = 8.12 Hz, 1H, arom. CH), 7.72 (t, J = 7.24 Hz, 1H, arom. CH), 8.07 (d, J = 7.88 Hz, 1H, arom. CH), 12.74 (s, 1H, NH, D_2O exchangeable); ^{13}C NMR (DMSO-d_6) δ ppm: 56.35 (2 OCH_3), 60.42 (OCH_3), 89.71 (C3, pyrazoloquinazoline), 105.38 (C2, C6, benzene),

112.99 (C8a, pyrazoloquinazoline), 116.47 (C5, pyrazoloquinazoline), 122.39 (C7, pyrazoloquinazoline), 127.39 (C8, pyrazoloquinazoline, C1, benzene), 134.98 (C6, pyrazoloquinazoline), 136.56 (methylidene carbon), 138.16 (C4, benzene), 139.82 (C4a, pyrazoloquinazoline), 142.42 (C3a, pyrazoloquinazoline), 153.05 (C3, C5, benzene), 153.11 (C9, pyrazoloquinazoline, C═O), 166.30 (C2, pyrazoloquinazoline, C═O); anal. calcd. for $C_{20}H_{17}N_3O_5$ (379.37): C, 63.32; H, 4.48; N, 11.08; found C, 63.59; H, 4.67; N, 11.20.

4.2 | Biological evaluation

4.2.1 | In vitro COX-1 and COX-2 inhibitory assay

COX-1 and COX-2 isozymes inhibition was evaluated using 10-fold serial dilutions (1, 0.1, 0.01, 0.001 μg/ml) according to manufacturer's instructions. Using the COX-1 (human) Inhibitor Screening Assay Kit and COX-2 (human) Inhibitor Screening Assay Kit (catalog numbers: 701070 and 701080, respectively, supplied by Cayman Chemical Company, Ann Arbor, MI), the color was measured with ROBONIK P2000 ELISA reader. The method is based on measuring $PGF_{2\alpha}$ produced from stannous chloride reduction of COX-derived PGH2 produced in the COX reaction, which is based on the competition between PGs and a PG-acetylcholinesterase conjugate (PG tracer) for a limited amount of PG antiserum.

The enzymes, COX-1 and COX-2 (10 μl), heme (10 μl), and samples (20 μl) were incubated for 10 min at 37°C with the supplied reaction buffer solution (160 μl, 0.1 M Tris-HCl, pH 8 containing 5 mM EDTA and 2 mM phenol). Then, COX reactions were initiated by the addition of arachidonic acid (100 μl), and the reaction was stopped after 30 s using stannous chloride. The $PGF_{2\alpha}$ formed in the samples by COX reactions was quantified by ELISA. After transfer to a 96-well plate, the plate was washed to remove any unbound reagent, and then Ellman's reagent (200 μl), which contains acetylcholinesterase substrate, was added and incubated at room temperature for 60–90 min until the absorbance of B_o well was in the range 0.3–0.8 A.U. at 410 nm. The plate was then read by an ELISA plate reader.

The percentage inhibition was calculated for the different concentrations tested against the control, and the IC_{50} values against both COX-1 and COX-2 enzymes were calculated from the concentration–inhibition curve.

4.2.2 | In vivo anti-inflammatory assay

Animals' treatment protocol was approved by the Faculty of Pharmacy, Cairo University, Animal Rights Committee (OC2085). In all tests, adequate considerations were adopted to reduce the pain or discomfort of animals. All quantitative results obtained from the biological evaluation were calculated as the mean ± standard error. The statistical significance between the data for celecoxib and test compounds was assessed by one-way analysis of variance ($p < .05$).

Male albino rats of Sprague Dawley strain, weighing 130–150 g,[44,45] were kept in the animal house unit of pharmacology and toxicology department for at least 1 week before the experiment under standard conditions of light and temperature. All animals were fed a standard laboratory diet consisting of vitamin mixture (1%), mineral mixture (4%), corn oil (10%), sucrose (20%), cellulose (0.2%), casein 95% pure (10.5%), and starch (54.3%). All test compounds were suspended in 10% Tween-80 solution in distilled water. According to a previously reported method,[46,47] the rats were marked and divided into six experimental groups of six rats each. The first group received 1 ml saline and served as the untreated control. The second to fourth group received 10 mg/kg of tested compounds **3f**, **3h**, and **3j**, respectively. The fifth and sixth groups received 10 mg/kg of the reference drugs celecoxib and indomethacin, respectively, and served as reference standards groups. After 1 hr of oral administration of all previous compounds, the right hind paw of each animal was injected by a subplantar injection of 0.1 ml of 1% carrageenan solution. The paw volume was recorded using a plethysmometer (UGO Basile 7140) at 0, 1, 2, 3, and 4 hr, and the percentage edema inhibition was calculated using the following equation: anti-inflammatory activity (%) = $(1 - D_t/D_c)/100$, where D_t represents the difference in paw volume before and after the drug was administered to the rats and D_c represents the difference of volume in the control groups.

4.2.3 | Gastric ulcerogenic activity

Rats were starved for 18 hr before the experiment and were divided into seven groups of six rats each, and the tested compounds, references (celecoxib and indomethacin), or saline as control were administered orally at a dose of 10 mg/kg body weight.[48] Then, 4 hr after the treatment, the animals were killed and their stomachs were removed and examined macroscopically using a magnifying lens. A longitudinal incision along the greater curvature was made with a fine scissor. The presence of single or multiple lesions, erosion, ulcer, or perforation was evaluated. The number of ulcers and the occurrence of hyperemia were noted. The gastric lesions were stretched out and scored from 0 (*no lesion*) to 5 (*three or more marked ulcers*), according to the method of Clementi et al.[49]

4.2.4 | Determination of rat serum PGE2

Rat serum levels of (PGs) PGE2 were determined using blood samples collected from the rats subjected to carrageenan rat paw edema model 4 hr after carrageenan injection, using a PGE2-specific enzyme immunoassay kit according to the manufacture's protocol (catalog number: 514010; Cayman Chemical). The optical density was determined after 1 hr using a microplate reader DYNATech, MR 5000 (Dynatech Industries Inc., McLean, VA) at 450 nm and expressed as pg/ml.

4.2.5 | In vitro 5-LOX inhibitory screening assay

The 5-LOX inhibitor screening assay was performed to assess the inhibitory effect of synthesized compounds using 5-Lipoxygenase Inhibitor Screening Kit (Fluorometric; BioVision, CA) according to manufacturer procedures (catalog number: K980-100). The assay depends on the recording fluorescence every 30 s and then ΔRFU for all the screened compounds, using Topotecan, USA, Spark 10 M, multimode microplate reader.[50]

4.2.6 | Effect of the Ca^{2+} ionophore A23187 on isolated PMNL from experimental rats

PMNL isolated from normal rats were classified into 13 groups, and each group was preincubated with 5 μM of the selected compounds for 15 min except the control group. All groups were further stimulated by incubation with 5 μM of Ca^{2+} ionophore A23187 at 37°C for 5 min in the presence of 1 mM $CaCl_2$. The reactions were stopped by the addition of a mixture of chloroform and methanol (1:2, v/v). The leukotrienes (LTB4) quantification were performed with an estimation of their UV absorbances after the separation with high-performance liquid chromatography. After the stimulation of PMNL by 5 μM A23187 for 5 min, 1 ml of the centrifugate was collected and 3 ml of ethyl acetate was added after centrifugation. The sample was acidified to pH 3.0 with HCl, and PGB2 (100 ng) was added to the sample as an internal standard. The sample was vortexed and the layer of ethyl acetate was assembled. Separation of LTB4 was performed on reverse-phase column (240 × 0.4 mm inner diameter, LiChrosorb RP-18; Merck). The mobile phase was acetonitrile, methanol, water, and acetic acid (350:150:250:1, v/v). The flow rate was 1 ml/min. LTB4 and PGB2 were monitored at 270 nm.[51]

4.3 | Molecular docking into the COX-2 and 5-LOX active sites

Molecular docking was performed with Accelrys Discovery Studio 4.5 software using the Dock Ligands (CDOCKER) protocol, which is an implementation of the CDOCKER algorithm. CDOCKER is a grid-based molecular docking method that employs a CHARMm-based molecular dynamics (MD) scheme to dock ligands into a receptor-binding site. Random ligand conformations are generated using high-temperature MD. This method allows docking of any number of ligands with a single protein receptor. The −CDOCKER_interaction_energy is the scoring function applied to the ligands. The poses were sorted by CHARMm energy, and the top scoring poses were calculated. The molecular docking was based on the crystal structures of COX-2 (PDB ID: 1CX2),[52] which is a crystal structure of cyclooxygenase-2 complexed with SC-558 (1-phenyl sulfonamide-3-trifluoromethyl-5-*p*-bromophenylpyrazole) and a crystal structure of 5-LOX enzyme co-crystallized with zileuton (PDB entry: 3O8Y),[53] downloaded from Protein Data Bank (PDB) website (https://www.rcsb.org/).

The protein was prepared using a prepare protein parameter that cleans up common problems in the input protein structure during preparation for further processing; it inserts and minimizes missing atoms in residue as hydrogen, and it also removes alternate conformations. All of the water molecules are removed.

CONFLICTS OF INTERESTS

The authors declare that there are no conflicts of interests.

ORCID

Khaled O. Mohamed http://orcid.org/0000-0002-2293-5363

REFERENCES

[1] X. de Leval, F. Julémont, J. Delarge, B. Pirotte, J.-M. Dogné, *Curr. Med. Chem.* **2002**, *9*, 941.
[2] S. Fiorucci, R. Meli, M. Bucci, G. Cirino, *Biochem. Pharmacol.* **2001**, *62*, 1433.
[3] C. D. Funk, *Science* **2001**, *294*, 1871.
[4] M. L. Capone, S. Tacconelli, L. Di Francesco, A. Sacchetti, M. G. Sciulli, P. Patrignani, *Prostaglandins Other Lipid Mediat.* **2007**, *82*, 85.
[5] R. A. Moore, S. Derry, L. S. Simon, P. Emery, *Pain Pract.* **2014**, *14*, 378.
[6] P. Patrignani, C. Patrono, *Biochim. Biophys. Acta, Mol. Cell Biol. Lipids* **2015**, *1851*, 422.
[7] C. Patrono, B. Rocca, *Pharmacol. Res.* **2009**, *59*, 285.
[8] R. G. Kurumbail, A. M. Stevens, J. K. Gierse, J. J. McDonald, R. A. Stegeman, J. Y. Pak, D. Gildehaus, T. D. Penning, K. Seibert, P. C. Isakson, *Nature* **1996**, *384*, 644.
[9] O. Llorens, J. J. Perez, A. Palomer, D. Mauleon, *Bioorg. Med. Chem. Lett.* **1999**, *9*, 2779.
[10] R. J. Flower, *Nat. Rev. Drug. Discov.* **2003**, *2*, 179.
[11] T. D. Penning, J. J. Talley, S. R. Bertenshaw, J. S. Carter, P. W. Collins, S. Docter, M. J. Graneto, L. F. Lee, J. W. Malecha, J. M. Miyashiro, *J. Med. Chem.* **1997**, *40*, 1347.
[12] M. A. Hussein, *Med. Chem. Res.* **2013**, *22*, 4641.
[13] Ş. G. Küçükgüzel, S. Şenkardeş, *Eur. J. Med. Chem.* **2015**, *97*, 786.
[14] E. Manivannan, S. C. Chaturvedi, *Bioorg. Med. Chem.* **2011**, *19*, 4520.
[15] S. Lee, J.-K. Son, B. Jeong, T.-C. Jeong, H. Chang, E.-S. Lee, Y. Jahng, *Molecules* **2008**, *13*, 272.
[16] T. C. Moon, M. Murakami, I. Kudo, K. H. Son, H. P. Kim, S. S. Kang, H. W. Chang, *Inflamm. Res.* **1999**, *48*, 621.
[17] H. Danz, S. Stoyanova, P. Wippich, A. Brattström, *Planta Med.* **2001**, *67*, 411.
[18] Y. Jahng, *Arch. Pharm. Res.* **2013**, *36*, 517.
[19] D. Wong, M. Wang, Y. Cheng, G. A. FitzGerald, *Curr. Opin. Pharmacol.* **2005**, *5*, 204.
[20] P. Ungprasert, N. Srivali, W. Kittanamongkolchai, *Eur. J. Intern. Med.* **2015**, *26*, 685.
[21] C. Scarpignato, A. Lanas, C. Blandizzi, W. F. Lems, M. Hermann, R. H. Hunt, *BMC Med.* **2015**, *13*, 55.
[22] M. A. Bray, A. W. Ford-Hutchinson, M. J. H. Smith, *Prostaglandins* **1981**, *22*, 213.
[23] J. F. Penrose, K. F. Austen, B. K. Lam, *Inflammation Basic Princ. Clin. Correl.* **1999**, 361.
[24] J. Martel-Pelletier, D. Lajeunesse, P. Reboul, J.-P. Pelletier, *Ann. Rheum. Dis.* **2003**, *62*, 501.
[25] A. Sala, G. M. Aliev, G. Rossoni, F. Berti, C. Buccellati, G. Burnstock, G. Folco, J. Maclouf, *Blood* **1996**, *87*, 1824.
[26] B. M. Peskar, *Gastroenterology* **1991**, *100*, 619.
[27] S. L. Manju, K. R. Ethiraj, G. Elias, *Eur. J. Pharm. Sci.* **2018**, *121*, 356.
[28] G. Moussa, R. Alaaeddine, L. M. Alaeddine, R. Nassra, A. S. F. Belal, A. Ismail, A. F. El-Yazbi, Y. S. Abdel-Ghany, A. Hazzaa, *Eur. J. Med. Chem.* **2018**, *144*, 635.

[29] A. Araico, M. C. Terencio, M. J. Alcaraz, J. N. Dominguez, C. León, M. L. Ferrándiz, *Life Sci.* **2006**, *78*, 2911.
[30] A. Araico, M. C. Terencio, M. J. Alcaraz, J. N. Dominguez, C. León, M. L. Ferrándiz, *Life Sci.* **2007**, *80*, 2108.
[31] B. Hofmann, S. Barzen, C. B. Rödl, A. Kiehl, J. Borig, A. Zivkovic, H. Stark, G. Schneider, D. Steinhilber, *J. Med. Chem.* **2011**, *54*, 1943.
[32] S. Sogawa, Y. Nihro, H. Ueda, A. Izumi, T. Miki, H. Matsumoto, T. Satoh, *J. Med. Chem.* **1993**, *36*, 3904.
[33] M. A. Shaaban, L. N. Soliman, S. M. A. Roshdy, K. O. A. Mohamed, *Bull. Fac. Pharm. (Cairo Univ.)* **2009**, *47*, 35.
[34] G. Mariappan, B. P. Saha, L. Sutharson, A. Haldar, *Indian J. Chem.* **2010**, *49B*, 1671–1674.
[35] A. Mandour, E. El-Sawy, M. Ebaid, S. Hassan, *Acta Pharm.* **2012**, *62*, 15.
[36] R. M. Silverstein, F. X. Webster, D. J. Kiemle, D. L. Bryce, Spectrometric Identification of Organic Compounds. 2014.
[37] H. ur Rashid, X. Yiming, N. Ahmad, Y. Muhammad, L. Wang, *Bioorg. Chem.* **2019**, *87*, 335.
[38] C. A. Winter, E. A. Risley, G. W. Nuss, *Proc. Soc. Exp. Biol. Med.* **1962**, *111*, 544.
[39] A. Ghith, K. M. Youssef, N. S. M. Ismail, K. A. M. Abouzid, *Bioorg. Chem.* **2019**, *83*, 111.
[40] J. Dietrich, C. Hulme, L. H. Hurley, *Bioorg. Med. Chem.* **2010**, *18*, 5738.
[41] E. V. Schneider, J. Böttcher, R. Huber, K. Maskos, L. Neumann, *Proc. Natl. Acad. Sci. U. S. A.* **2013**, *110*, 8081.
[42] D. De Lucia, O. M. Lucio, B. Musio, A. Bender, M. Listing, S. Dennhardt, A. Koeberle, U. Garscha, R. Rizzo, S. Manfredini, *Eur. J. Med. Chem.* **2015**, *101*, 573.
[43] S. B. Ganorkar, Y. Vander Heyden, A. A. Shirkhedkar, D. K. Lokwani, D. M. Dhumal, P. S. Bobade, *J. Pharm. Biomed. Anal.* **2019**, *179*, 112982.
[44] M. Koksal, I. Ozkan-Dagliyan, T. Ozyazici, B. Kadioglu, H. Sipahi, A. Bozkurt, S. S. Bilge, *Arch. Pharm.* **2017**, *350*, e1700153.
[45] E. M. Ahmed, A. E. Kassab, A. A. El-Malah, M. S. A. Hassan, *Eur. J. Med. Chem.* **2019**, *171*, 25.
[46] T. H. Ibrahim, Y. M. Loksha, H. A. Elshihawy, D. M. Khodeer, M. M. Said, *Arch. Pharm. Chem. Life Sci.* **2017**, *350*, e1700093.
[47] L. W. Mohamed, M. A. Shaaban, A. F. Zaher, S. M. Alhamaky, A. M. Elsahar, *Bioorg. Chem.* **2019**, *83*, 47.
[48] E. M. Ahmed, M. S. A. Hassan, A. A. El-Malah, A. E. Kassab, *Bioorg. Chem.* **2020**, *95*, 103497.
[49] G. Clementi, A. Caruso, V. M. C. Cutuli, E. de Bernardis, A. Prato, N. G. Mangano, M. Amico-Roxas, *Eur. J. Pharmacol.* **1998**, *360*, 51.
[50] B. Roschek Jr, R. C. Fink, D. Li, M. McMichael, C. M. Tower, R. D. Smith, R. S. Alberte, *J. Med. Food* **2009**, *12*, 615.
[51] Y. Nakagawa, E. Ishii, *Biochim. Biophys. Acta, Mol. Basis Dis.* **1996**, *1315*, 145.
[52] Y. Dai, K. Hartandi, Z. Ji, A. A. Ahmed, D. H. Albert, J. L. Bauch, J. J. Bouska, P. F. Bousquet, G. A. Cunha, K. B. Glaser, *J. Med. Chem.* **2007**, *50*, 1584.
[53] N. C. Gilbert, S. G. Bartlett, M. T. Waight, D. B. Neau, W. E. Boeglin, A. R. Brash, M. E. Newcomer, *Science* **2011**, *331*, 217.

SUPPORTING INFORMATION

Additional supporting information may be found online in the Supporting Information section.

How to cite this article: Shaaban MA, Kamal AM, Faggal SI, et al. Design, synthesis, and biological evaluation of new pyrazoloquinazoline derivatives as dual COX-2/5-LOX inhibitors. *Arch Pharm*. 2020;353:e2000027. https://doi.org/10.1002/ardp.202000027